Photolysis of hydrogen chloride embedded in the first argon solvation shell: Rotational control and quantum dynamics of photofragments

Petra Žďánská
J. Heyrovský Institute of Physical Chemistry, Academy of Sciences of the Czech Republic, Dolejškova 3, 18223 Prague 8, Czech Republic

Burkhard Schmidt
Institut für Physikalische und Theoretische Chemie, WE 3, Freie Universität Berlin, Takustrasse 3, D-14195 Berlin, Germany

Pavel Jungwirth[a)]
J. Heyrovský Institute of Physical Chemistry, Academy of Sciences of the Czech Republic, Dolejškova 3, 18223 Prague 8, Czech Republic

(Received 14 October 1998; accepted 21 December 1998)

Under standard conditions reaction yields are connected with terms like free energy differences and thermal distributions. However, many modern experimental techniques, such as supersonic beam expansion or matrix isolation, deal with cryogenic temperatures and isolated reactants in inert clusters or solid matrices. Under these conditions the photochemical reaction mechanism is in many cases strongly dependent on the shape of delocalized initial vibrational or rotational wave functions of the reactants which can be employed for an efficient reaction yield control. Here, we apply, using quantum molecular dynamics simulations, such a scheme to the rotational control of photolysis of the HCl molecule embedded in an icosahedral Ar_{12} cluster. First, the HCl molecule is preexcited into a specific low lying rotational level. Depending on the rotational state, the hydrogen probability is enhanced in different directions within the cluster. In a second step, the HCl molecule is photolyzed by an UV pulse. The rapidly dissociating hydrogen atom then reaches primarily either the holes in the solvent shell or the argon atoms, depending on the rotational preexcitation. Starting either from the ground or from the first totally symmetric excited rotational states, the direct dissociation and the delayed process accompanied by a temporary trapping of the hydrogen atom have very different relative yields. As a consequence, differences up to a factor of 5 in the temporary population of the hydrogen atom inside the cluster after the first hydrogen-cage collision are observed. In the energy domain a significant difference in the structure of the kinetic energy distribution spectra, connected with the existence of short-lived vibrational resonances of the hydrogen atom, is predicted. [S0021-9606(99)51012-X]

I. INTRODUCTION

Hydrogen halide molecules solvated in rare gas clusters and matrices serve as prototype systems for the study of solvation of diatomics in an inert environment. Among the most intensively investigated systems are the hydrogen chloride and hydrogen fluoride molecules in argon clusters and in solid argon. High resolution far-IR and microwave spectroscopic measurements have been performed for the smallest clusters in this family providing detailed and accurate information about their rovibrational structure and interactions.[1–11] A lot of emphasis has been directed toward elucidating the process of sequential solvation. Namely, structures of $HX(Ar)_n$ (X=F, Cl, or Br, $n=1,...,12$) clusters have been investigated and HX vibrational line shifts have been measured and calculated starting from a single solvent atom up to the matrix environment.[6,12–18] It has been shown that $HX(Ar)_n$ clusters can exist in several isomers and a competition between bulk and surface solvation of the hydrogen halide has been observed in larger clusters.[6] In addition, data from high resolution far-IR and microwave measurements have been used for a construction of very accurate ground electronic state interaction potentials for these systems.[7,8,19]

While there is ample information concerning the $HX(Ar)_n$ systems in their ground electronic state, several studies also have investigated the dynamical processes connected with the UV excitation of the HX chromophore into the first dissociation continuum. The typical questions addressed in this context concern the role of the inert cluster or matrix in caging, i.e., in hindering mainly the motion of the photodissociating highly energetic hydrogen atom, and in fragmentation and rovibronic relaxation processes.[20–28,27,29–33]

One of the most exciting features of hydrogen halide molecules in their ground electronic state solvated in a cryogenic rare gas environment is the large amplitude motion of the hydrogen atom perpendicular to the HX molecular axis. The cold and light hydrogen atom in a shallow intermolecular potential behaves as a strongly delocalized quantum particle. Depending on the concrete system, particularly on the number of solvent atoms and the solvation site, hydrogen

a)Electronic mail: jungwirt@jh-inst.cas.cz

motions ranging from a large amplitude bending (e.g., for the collinear Ar...HX cluster) to an almost free rotation (e.g., for the HX molecule inside large argon clusters or matrices) have been observed[24,30,34,35]. Not only is the hydrogen motion strongly delocalized but there are also large differences in the spatial hydrogen density between the ground and low-lying excited (hindered) rotational states.[8,33,36]

In this paper we provide for the HCl molecule immersed in an icosahedral first solvation shell of 12 argon atoms a unified and consistent quantum mechanical picture of both the electronic ground state rotational and vibrational structure and of the photodissociation dynamics on the first excited electronic surface. The principal goal of this study is to show that the process of hydrogen halide photodissociation in a rare gas environment can be efficiently influenced and controlled by a preexcitation of the system to a given (hindered) rotational state using, e.g., multiphoton or Raman excitation. In particular, it is shown for the system under investigation that specific totally symmetric excited rotational states have large hydrogen probability toward the holes in the argon cage which enhances the direct dissociation process, while other excited rotational states prefer the hydrogen atom to point toward the argons, which is favorable for a temporary trapping of the dissociating hydrogen. The idea presented in this paper is loosely connected to the vibrational control scheme pursued by several groups in the last two decades.[37–42] Unlike the other investigators who typically preexcite stiff stretching vibrational modes, the method proposed here consists in controlling the photodissociation process by preexciting an almost free rotational mode.

The possibility to control photochemical processes by rotational preexcitation is not limited to the particular system investigated in this paper. The key ingredients for an efficient control are large amplitude rotational or hindered rotational motions and low temperatures, ensuring good state specificity and large spatial differences between the individual rotational wave functions. The latter condition means performing experiments, e.g., using supersonic jet expansion or in cryogenic matrices. The former condition is fulfilled by practically all weakly bound complexes involving hydrogen-containing molecules. In our previous studies, we have shown that an efficient control does not require an almost free rotation.[36,43] For enhancing the yield of a photochemical process by a factor of 2–30 (depending on a particular system) by far-IR preexcitation it suffices that a large amplitude bending (librational) motion is present as in the case of the Cl...HCl complex[43] or surface solvated HCl on a large $Ar_{12}Cl$ cluster.[36] The Cl...HCl cluster is an example of hydrogen-bonded complexes, an indication that this very important class of systems can be subjected to rotational/librational control. Finally, we note that the proposed scheme is not limited to diatomic host molecules and, e.g., water and its isotopes are currently being investigated in our group.

The paper is organized as follows. The system under investigation and the underlying potential energy surfaces are introduced in Sec. II. In Sec. III we describe the methods used for the construction of the initial quantum states of the system and for the photodissociation wave packet dynamics together with computational details. Results and discussion are presented in Sec. IV and Sec. V contains the concluding remarks.

II. SYSTEM AND POTENTIALS

A. Geometry and symmetry

As is known from theory[44] and from electron diffraction experiments,[45] argon clusters of up to a few thousands of atoms acquire icosahedral geometry. The system studied here is the HCl molecule surrounded by a ''magic'' number of 12 argon atoms forming an icosahedral first solvation layer. The HCl molecule is slightly too large to fit into the central position of the cluster. This is a well-known feature studied thoroughly via vibrational shifts in the HCl vibrational spectrum in argon clusters of different sizes.[18] However, the potential barriers of the hindered rotation are small enough to allow for an almost free rotation of the hydrogen atom in the cage even in the lowest rotational states (see Sec. IV for more details).

It has recently been pointed out that in addition to the fully solvated HCl there exists a surface isomer of $HClAr_{12}$ which is even slightly more stable.[6] The relative abundance of these isomers depends on the particular experimental conditions of the mixed cluster formation, e.g., by supersonic jet expansion.

B. Potentials

The ground electronic state potential is approximated by an accurate three-body (atom–diatom) potential for the HCl interaction with an argon atom[46] and by pair potentials for the remaining interactions. The pair interaction between hydrogen and chlorine is approximated by a Morse potential.[47] The argon–argon pair interaction is modeled by the HFD-B potential.[48]

We assume the HCl molecule to be excited by a short laser pulse promoting it from the $^1\Sigma$ to the $^1\Pi$ state where it dissociates.[49] For the electronically excited state of the whole system, we construct a potential energy surface using a diatomics-in-molecule Hamiltonian[28] in which the anisotropy of the argon–chlorine potential caused by the unpaired electron of the chlorine atom is taken explicitly into account.[50] The remaining interactions are approximated by pair potentials. The hydrogen–chlorine pair potentials for both the $^1\Sigma$ and the $^1\Pi$ states are taken from *ab initio* calculations[51] and are interpolated by cubic splines. The argon–argon pair interaction is the same as that used for the description of the ground state.

The processes of caging and cage exit are very sensitive to the character of the argon–hydrogen potential in the repulsive region. Existing Ar–H potentials were constructed with emphasis on the region of the van der Waals minimum.[52–55] In our simulations of the photodissociation dynamics the kinetic energy of the hydrogen atom hitting the cage is up to 4 eV, which shifts our interest to the strongly repulsive part of the potential energy curve. This region from about 1.5 to 3 Å has not been described accurately yet. Therefore, we have performed high level *ab initio* calculations to map the whole potential with a sufficient degree of accuracy. The coupled-cluster single double triple CCSDT

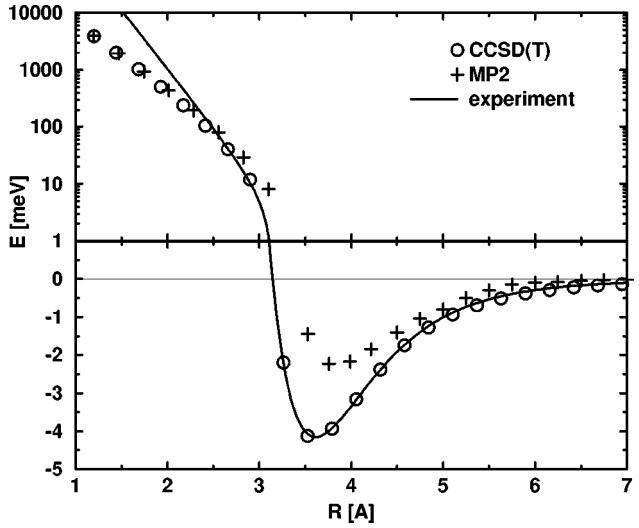

FIG. 1. Ar–H potential energy curves. The curves labeled MP2 and CCSDT represent *ab initio* calculations of the present work. The experimental potential energy curve is based on measured differential scattering cross sections of Ref. 52 which also reproduce the integral cross sections of Ref. 59.

method with Dunning augmented quadruple-zeta basis set (aug-cc-pVQZ) has been employed.[56–59] We have found that the coupled cluster method with such an extended basis set provides practically basis set superposition error free and converged results for the system under study. Finally, we note that the CCSDT and also lower level second-order Moller–Plesset (MP2) energy evaluations are based on an unrestricted open-shell Hartree–Fock wave function. There is always a potential danger when using unrestricted wave functions that higher spin states may mix and spoil the quality of the results. However, this is not the case for the Ar–H system where the expectation values of S^2 for the unrestricted wave function lie in the interval (0.750–0.754) for the whole investigated range of interatomic separations and the wave function is, therefore, practically of a pure doublet character.

The resulting Ar–H potential is presented in Fig. 1. Figure 1 shows a comparison of the CCSDT/aug-cc-pVQZ results with lower level MP2/aug-cc-pVTZ calculations and with a curve obtained by fitting to measured differential[53] and integral[60] cross sections. While the two *ab initio* curves agree very well in the strongly repulsive region, the MP2 method underestimates the van der Waals well depths. The CCSDT calculations (without any adjustment or shifting of the potential) practically coincide with the experiment in the van der Waals region while being less repulsive at very short internuclear separations. However, this difference is within the uncertainty of the fit to the experimental data.[52] Since our calculations are well converged especially in the repulsive region both in method and basis set we consider the potential presented here to be very reliable and most suitable for the description of the process under study.

We have evaluated 35 CCSDT/aug-cc-pVQZ energy points in the range of Ar–H distances from 1.2 to 10 Å and for the dissociation limit. In the dynamical calculations we use an exponential expression (in atomic units)

$$V_{\mathrm{Ar-H}} = 2.6456 e^{-1.1868r - 0.040\,835r^2}, \tag{1}$$

which perfectly fits the *ab initio* points in the repulsive part of the potential. Since the photodissociating hydrogen atoms have several electron volts of excess energy this is the only part which is relevant for our dynamical study. More precisely, as is shown later, even the slowest fraction of the hydrogens temporarily trapped in the cluster leave the cage with more than 2 eV of kinetic energy, which is 2.5 orders of magnitude larger than the Ar–H binding energy. The temporary trapping is, therefore, due to multiple repulsive collisions and not to the extremely weak Ar–H attraction which can be safely neglected. Note also that at short internuclear separations the present potential curve is less repulsive than the (semi)empirical H–Ar potentials[52–54,60] used in previous studies of $HClAr_n$ photodissociation.

For sake of feasibility of quantum dynamical calculations of the large $HCl@Ar_{12}$ system we constrain ourselves to an approximation which neglects the effect of the spin–orbit coupling connected with the open-shell Cl atom. We do not consider the possibility of nonadiabatic transitions between the electronic states involved. While spin–orbit coupling and nonadiabatic effects are found to be important for longer time dynamics of the HCl molecule in very large argon clusters and matrices, their influence is minor for the ultrafast HCl photodissociation process in the $HCl@Ar_{12}$ cluster, especially in comparison with the rotational control effect which is in the focus of the present study.[27,28]

III. METHOD

A. Choice of coordinates

The physics of the process under study directly prompts us to divide the problem into the description of the fast hydrogen motion on the one side and the slow motion of heavy atoms on the other side. Therefore, we choose coordinates for the motion of the hydrogen atom separate from coordinates of the heavy atoms of the cluster. In particular, we employ spherical coordinates for the HCl molecule and normal modes for argon atoms and the center of mass of the HCl diatomic. Since the Cl atom is 35 times heavier than the H atom, it sits almost at the center of mass of the HCl molecule. For this reason, we often refer in this paper to the HCl inner coordinates as to the coordinates of the hydrogen motion. In our nomenclature we, moreover, for sake of simplicity, refer to the motion of the argons plus the motion of the center of mass of the HCl molecule as cage motions.

For the construction of normal modes of the cage we use a quantum description of hydrogen rotations while the remaining coordinates of the nuclei undergo a classical minimization procedure followed by construction and diagonalization of the Hessian matrix. Such a procedure is well justified for the ground electronic state where the rotation of the hydrogen atom is well separated from other coordinates. The quantum description of the two-dimensional hydrogen rotation has already been developed earlier for this system[30,34] and is briefly summarized in Sec. IV A 1. The two-dimensional hydrogen rotational wave function is used to evaluate the effective potential as a function of the cage coordinates, the H–Cl distance, and the rotational number.

The assumed separation of the HCl rotation in the ground electronic state and the cage modes (i.e., the neglect of the rotational–translational coupling) is further supported by rotational spectra of matrix isolated HCl molecule which show only a very weak perturbance from the free rotor spectrum.[61,62]

B. Initial wave function

The initial separability of hydrogen rotation and vibration is assumed together with the initial separability between the hydrogen and cage modes. The vibrational ground state of the cage is constructed in the harmonic approximation. The initial wave function Ψ_0 of the system then reads

$$\Psi_0(q_1,\ldots,q_{33},\rho,\phi,\theta)\propto e^{(-(1/2)\omega_1 q_1^2)}\ldots e^{(-(1/2)\omega_{33} q_{33}^2)} \times\frac{\Phi_{\mathrm{vib}}(\rho)}{\rho}\Phi_{\mathrm{rot}}(\phi,\theta) \tag{2}$$

where q_i are the normal coordinates of the cage, ρ,ϕ,θ are internal spherical coordinates of the HCl molecule, and ω_i are the angular frequencies of the cage modes. The Morse ground vibrational wave function Φ_{vib} of the HCl molecule is divided by ρ, which comes from the use of spherical coordinates. The initial rotational state Φ_{rot} of the HCl molecule is taken either as a ground or low-lying totally symmetric (A_g) excited state, which establishes the rotational control, discussed in detail later. The choice of only totally symmetric rotational functions has two reasons. First, it turns out that the rotational control is most efficient for A_g states. Second, this restriction, which leads to a much smaller rotational basis, grossly speeds up the numerically very demanding calculations.

C. Dynamics upon photoexcitation: Quantum-classical molecular dynamics

Since a fully quantum-mechanical treatment of the dynamics of a system comprised of 14 atoms is far beyond present computational means, we employ two different levels of approximation which are presented here and in Sec. III D. The first model to describe the photodissociation dynamics of the $HCl@Ar_{12}$ system is the quantum-classical molecular dynamics (QCMD) scheme which was introduced into the field of chemical physics some 20 years ago.[63] Recently, detailed investigations of the approximation properties have also been published.[64,65]

Based on the disparity of masses between the light (H) and the heavy (Cl, Ar) atoms involved, the basic idea of the QCMD scheme is to split the complete system into a quantum-mechanical and classical subsystems. For the light particle a three-dimensional wave function $\psi(\rho,\theta,\phi)$ is propagated subject to the Schrödinger equation

$$i\hbar\frac{\partial}{\partial t}\psi=(\hat{T}_{\mathrm{qm}}+\hat{V}_{\mathrm{qm}})\psi, \tag{3}$$

where $\hat{T}_{\mathrm{qm}}$ is the kinetic operator in spherical coordinates and $\hat{V}_{\mathrm{qm}}$ is the potential energy operator specified below. For the positions $\mathbf{q}$ and momenta $\mathbf{p}$ of the heavy particles we solve Hamilton equations of motion for each mode i,

$$\frac{\partial q_i}{\partial t}=\frac{\partial(T_{\mathrm{cl}}+V_{\mathrm{cl}})}{\partial p_i}, \tag{4}$$

$$\frac{\partial p_i}{\partial t}=-\frac{\partial(T_{\mathrm{cl}}+V_{\mathrm{cl}})}{\partial q_i}, \tag{5}$$

where T_{cl} is the kinetic energy of the mass-scaled normal mode coordinates. The dynamics of the two subsystems are coupled self-consistently through effective (time-dependent) potentials: The potential V_{qm} for the quantum-mechanical system is obtained from the full potential $V(\mathbf{q},\rho,\theta,\phi)$ by inserting the positions $\mathbf{q}(t)$ of the heavy atoms at every instant of time. Conversely, the mean-field potential $V_{\mathrm{cl}}=\langle\psi|V(\mathbf{q},\rho,\theta,\phi)|\psi\rangle_{\rho\theta\phi}$ for the classical part is the expectation value of the total potential with respect to the hydrogenic wave function.

D. Dynamics upon photoexcitation: Quantum representation of all modes

An alternative to the QCMD approach is an approximate description of the quantum dynamics of *all* modes. Methods for multidimensional quantum dynamics based on classical potentials[66–68] employed here use the quantum wave packet apparatus, however, they substitute quantum evaluations of effective single-mode potentials by a semiclassical averaging over Wigner trajectories.[69,70] The best established method from this family is the classical separable potential method (CSP), which uses the mean-field approximation.[66]

The CSP scheme, described in detail elsewhere,[66] consists of the following four steps:

(i) mapping the initial wave function onto a set of classical coordinates and momenta,
(ii) propagation of a set of classical trajectories,
(iii) construction of the time-dependent CSP potentials,
(iv) quantum one-dimensional propagations for each mode using the CSP potentials.

Let us elaborate in more detail on these steps. Since the classical trajectories should mimic the quantum evolution as well as possible, their initial conditions should correspond to the initial quantum wave function. This is accomplished by mapping the initial wave function $\Psi(\mathbf{q},0)$ of the whole system onto a weighted set $P_w(\mathbf{q},\mathbf{p})$ of initial coordinates and momenta using Wigner distribution.[69,71]

Once the initial coordinates, momenta, and weights are generated, a swarm of classical trajectories is propagated by numerically solving the Newton equations of motion in a standard way.[72] The number of trajectories needed for providing converged effective potentials depends on the particular process under study, size of the system, initial wave function, and duration of the simulation. Typically, 100–1000 trajectories are necessary for systems with tens to hundreds of atoms, which represents a relatively simple computational task.

In the next step, a time-dependent classical separable potential $\overline{V}^{\mathrm{CSP}}$ is evaluated for each mode j:

$$\overline{V}_j^{\mathrm{CSP}}(q_j,t)=\sum_{\alpha=1}^{n_T} V(q_1^{(\alpha)}(t),\ldots,q_{j-1}^{(\alpha)}(t),q_j,q_{j+1}^{(\alpha)} \times(t),\ldots,q_N^{(\alpha)}(t))\omega_\alpha+\frac{1-N}{N}\overline{V}(t), \tag{6}$$

where $V(q_1,\ldots,q_N)$ is the full potential function of the system, $\omega_\alpha=P_w(\mathbf{q}^\alpha,\mathbf{p}^\alpha)$ is the Wigner weight of the trajectory α in the initial state distribution, and the summation in Eq. (5) extends over all MD trajectories. The time-dependent energy normalization factor $\overline{V}(t)$ is given as

$$\overline{V}(t)=\sum_{\alpha=1}^{n_T} V(q_1^{(\alpha)}(t),\ldots,q_j^{(\alpha)}(t),\ldots,q_N^{(\alpha)}(t))\omega_\alpha. \tag{7}$$

Finally, the time-dependent Schrödinger equation

$$i\hbar\frac{\partial\phi_j(q_j,t)}{\partial t}=[T_j+\overline{V}_j^{\mathrm{CSP}}(q_j,t)]\phi_j(q_j,t) \tag{8}$$

is numerically solved for each mode j.

The large dynamical intermode correlations connected with the motion of the photodissociating hydrogen atom necessitate a more accurate description of the hydrogen wave function going beyond separability. Therefore, as in the previous QCMD simulations, a three-dimensional nonseparable wave function for the HCl inner degrees of freedom is used in order to correctly model the strong couplings between the rotational degrees of freedom θ,ϕ and the dissociative coordinate ρ. Thus, the three-dimensional hydrogenic motion is treated fully quantally in a numerically exact way while the other degrees of freedom are described by single-mode wave functions.

Now, let us discuss the separability of the hydrogenic coordinates and the cage modes. In general, mean-field approximations work best for the description of couplings caused by localized nodeless wave functions.[64,73] This is the case of the cryogenic cage wave functions which are initially the $v=0$ Gaussians. Due to the separation of masses and time scales between the hydrogen and the cage, the cage wave functions do not significantly evolve during the first $\approx$100 fs, which is the time necessary for the hydrogen to exit from the cage. Therefore, the mean-field approximation satisfactorily describes the influence of the cage on the fast hydrogenic motion.

On the other hand, the hydrogenic wave function is delocalized and for excited rotational states has a rich nodal pattern from the very beginning. Even more important, due to the highly energetic photodissociation process further delocalization and ''nodalization'' in the radial coordinate builds up very early. Therefore, the CSP method fails to quantitatively describe the energy transfer from the hydrogen to the cage during the photolysis. This is to a large extent rectified by employing a nonseparable version of the CSP method, which is described in more detail elsewhere.[67,73] Briefly, a separable wave packet is propagated along each classical trajectory instead of propagating a single wave packet along a potential obtained by averaging over all trajectories. Observable quantities such as kinetic excitations of individual cage modes are then obtained by averaging over all these separable wave packets *ex post* (the so called post-averaging procedure[67]).

For the propagation of both the hydrogen and cage wave functions Wigner trajectories have to be constructed for the evaluation of the effective potentials. The initial coordinates and momenta for the swarm of trajectories are determined from the Wigner distribution.[69,71,74] Substituting the initial wave function [see Eq. (1)] into the formula for the Wigner distribution we obtain the following relation for the initial quasiprobabilities:

$$P(q_1,\ldots,q_{33},\rho,\phi,\theta,p_1,\ldots,p_{33},p_\rho,J_z,p_z\rho) \propto e^{-\omega_1(q_1^2+p_1^2)}\cdots e^{-\omega_{33}(q_{33}^2+p_{33}^2)} \times\frac{P^{\mathrm{HCl,vib}}(\rho,p_\rho)}{\rho^2}P^{\mathrm{HCl,rot}}(\phi,\theta,J_z,p_z\rho). \tag{9}$$

Here, P is the quasiprobability for a trajectory with given initial conditions, p_i is the momentum coordinate of a cage mode i, p_ρ is the momentum in the HCl vibrational coordinate, J_z and $p_z\rho$ are conjugated momenta to the polar angles ϕ and θ, respectively. J_z is the projection of the total angular momentum onto the z axis, and $p_z\rho$ is the momentum in the z axis multiplied by the radius. $P^{\mathrm{HCl,vib}}$ and $P^{\mathrm{HCl,rot}}$ are the Wigner quasiprobabilities for the inner degrees of freedom of the HCl molecule.

The exact rotational Wigner distribution $P^{\mathrm{HCl,rot}}$ is a four-dimensional function of angular coordinates and the two conjugated momenta. For the ground rotational state the quasiprobability $P^{\mathrm{HCl,rot}}$ is a constant in angular coordinates and a Kronecker δ function at zero in the conjugated momenta. In the case of excited rotational states the rotational Wigner distributions acquire extremely complicated patterns in all four dimensions. It becomes computationally hardly feasible to sample the Wigner functions of higher rotational states with strongly oscillatory quasiprobabilities by a sufficient number of classical trajectories. Instead of the exact Wigner rotational distribution $P^{\mathrm{HCl,rot}}$ an approximate sampling of the angular wave function is, therefore, used. The initial spatial coordinates sample the shape of the wave function properly. This is crucial for a correct description of the rotational control mechanism since the initial hydrogen position decides whether the photodissociation process for the particular trajectory is direct or not and also determines the extent of caging. The role of the initial angular momenta for low-lying rotational states is much less important, therefore, their magnitudes are chosen simply to satisfy the condition of correct quantum rotational energy. This approximation is well justified by the fact that for the rotational states under study the initial angular kinetic energies of $\sim$0.1 eV are much smaller than the kinetic energy of roughly 3 eV gained during the early photodissociation (before the collision with the cage). Therefore, the collision dynamics is determined by the spatial hydrogen distribution, which is sampled accurately, and by the kinetic energy, which is dominantly the result of the photodissociation process. Finally, the directions of the angular momenta are sampled randomly, which is a good approximation for the highly symmetric icosahedral group.

E. Computational details

1. Quantum representation of the hydrogen atom wave function

The three-dimensional hydrogen wave function is represented in spherical coordinates. It is expanded in the following series:

$$\psi(\rho,\theta,\phi,t)=\sum_{J,N}\frac{\chi_{JN}^{(A_g)}(\rho,t)}{\rho}Z_{JN}^{(A_g)}(\theta,\phi), \tag{10}$$

where Z are the symmetry adapted (for the icosahedral group) spherical harmonics belonging to the totally symmetric representation A_g. Substituting this representation into the time-dependent Schrödinger equation results in a set of coupled equations governing the evolution of the functions χ. The excess energy of the photodissociating hydrogen is 3.8 eV, therefore the number of grid points for the dissociation coordinate and the number of rotational basis functions for the coupled angular coordinates of the hydrogen have to be sufficiently large. For the dissociation coordinate a grid of 1024 points in the region from 0.25 to 15 Å is used. A cubic optical potential is added in the region from 10 to 15 Å (which is far enough from the reactive region) in order to absorb the outgoing parts of the hydrogen wave packet. For the angular coordinates a basis set of spherical harmonics adapted to the totally symmetric irreducible representation (A_g) of the icosahedral point group (I_h) consisting of 147 functions with the main rotational number up to $J=124$ is used. The potential energy function is also expanded in terms of a reduced set of these functions and the resulting integrals over products of three spherical harmonics are evaluated using Clebsch–Gordan coefficients. For evaluation of the potential on the dense grid of the hydrogenic wave function a spline interpolation between accurately calculated points on a more sparse grid is used.

2. Quantum-classical molecular dynamics

The QCMD equations (see Sec. III C) are solved using a time-reversible second-order splitting scheme where the quantum-mechanical (ψ) and classical $(\mathbf{q},\mathbf{p})$ subsystems are propagated simultaneously $(\psi_0,\mathbf{q}_0,\mathbf{p}_0\rightarrow\psi_1,\mathbf{q}_1,\mathbf{p}_1)$ by a time step τ in the following way:[75]

$$\psi_{1/2}=\exp\left(-i\frac{\tau}{2\hbar}[T_{\mathrm{qm}}+V_{\mathrm{qm}}(\mathbf{q}_0)]\right)\psi_0,\quad \mathbf{q}_{1/2}=\mathbf{q}_0+\frac{\tau}{2}\mathbf{p}_0,$$

$$\mathbf{p}_1=\mathbf{p}_0-\langle\psi_{1/2}|\nabla_{\mathbf{q}}V(\mathbf{q}_{1/2})|\psi_{1/2}\rangle, \tag{11}$$

$$\mathbf{q}_1=\mathbf{q}_{1/2}+\frac{\tau}{2}\mathbf{p}_1,\quad \psi_1=\exp\left(-i\frac{\tau}{2\hbar}[T_{\mathrm{qm}}+V_{\mathrm{qm}}(\mathbf{q}_1)]\right)\psi_{1/2}.$$

Note that the propagation of the classical variables $\mathbf{q}$ and $\mathbf{p}$ is essentially equivalent to the classical Verlet algorithm[72] but it employs mean field forces which are obtained using the Hellman–Feynman theorem as expectation values of the forces $\nabla_{\mathbf{q}}V$ with respect to the hydrogenic wave function.[64,75] The first and the last steps of the above algorithm correspond to a half-step propagation of the quantum-mechanical wave packet subject to a Hamiltonian that depends on the positions of the classical particles. These propagations are realized by expanding the exponential of the time evolution operator in a series of complex Chebychev polynomials, thus permitting time steps which are typically much longer than periods of quantum-mechanical phase oscillations.[76] Consequently, the size of the time step is limited by the classical subsystem and can be chosen to be as large as 1 fs for the system considered here. Hence, the above integrator presents an alternative to multiple time step integrators.[77,78]

3. Quantum representation of all modes

In the spirit of classical potential methods (see Sec. III D) the three-dimensional effective potential for the hydrogen is evaluated using averaging over 50 Wigner trajectories. The effective potentials are reevaluated each 40 steps and a linear interpolation is used in between. The split propagator[79] with a time step of 0.025 fs is employed. The application of the three-dimensional split operator for the HCl propagation involves a diagonalization of a large matrix with a size equal to the number of rotational basis functions. The propagation is continued until the hydrogen entirely leaves the cluster, i.e., for 100–150 fs after the photoexcitation, depending on the initial rotational state of the HCl molecule.

The description of the cage modes is not extremely demanding on the density of the grid points for the following two reasons: The cage motions are spatially confined and the excitations of individual cage modes are moderate. The number of grid points employed is 256 for all coordinates. The grid sizes are in the interval from 7.5 to 20.0 in mass weighted atomic units. A sufficient number of trajectories which sample the highly delocalized hydrogen wave function is very important for a good description of the influence of the hydrogen motion on the cage dynamics. A calculation using 1000 trajectories is found to be converged for all practical purposes.

IV. RESULTS AND DISCUSSION

A. Initial wave function

1. Initial rotational wave function of the HCl molecule

The initial rotational functions are calculated in the basis of symmetry adapted functions of the free rotor. An analytical algorithm is used for the construction of the symmetry adapted basis set.[80,81] Clearly, the first basis function is the isotropic ground state function $J=0$ of the free rotor. The rotational functions with main rotational numbers from one up to five do not provide any icosahedral totally symmetric linear combination, so the second lowest symmetry adapted linear combination correlates with the main rotational number $J=6$. Next symmetry adapted linear combinations correlate with main rotational quantum numbers $J=10$, 12, 16, 18, 20, 22, 24, 26, and 28. Note, that there is no degeneracy for these rotational numbers, and the first doubly degenerate symmetrically adapted function correlates only with the main rotational number $J=30$. It is obvious that the use of the icosahedral symmetry significantly reduces the basis set which is computationally extremely important.

The barriers for rotation of HCl inside the icosahedral Ar_{12} cluster are equal to $32.6\,\mathrm{cm}^{-1}$. On the one hand this is

about three times the rotational constant of the free HCl molecule, on the other hand this is more than ten times less than the kinetic energy of the second totally symmetric $J=6$ function ($447.8\,\mathrm{cm}^{-1}$) which is the first one to mix within the totally symmetric irreducible representation. As a consequence of the weakness of this hindrance, the rotational states have at least a 99.9% overlap with the corresponding free rotor states.

The lowest excited hydrogen rotational wave functions in the cluster develop nodal patterns with large spatial differences in the probability density (see Fig. 2). At the same time, these rotational wave functions are highly delocalized around the whole sphere. Due to low rotational excitations implying a small number of nodes the structures in the wave functions are of the size of the interatomic distances in the cluster, which is important for an efficient rotational control.

The shape of the rotational wave function can be expected to predetermine to a large extent the dynamics following the HCl photolysis. Note that the anisotropic distribution of the hydrogen atom is preferentially oriented toward the cage atoms in the case of the $J=6$ state and toward the holes in the cage in the case of the $J=10$ state (see Fig. 2). The probability of the hydrogen to collide with the cage atom is therefore enhanced by the rotational preexcitation to the $J=6$ state, while being suppressed by the preexcitation to the $J=10$ state.

2. Initial wave function of the cage

For the three lowest totally symmetric rotational states of the hydrogen atom the cage geometry is optimized and the normal modes are constructed. Almost no differences between the three geometries are found. The geometry is also compared with the cage without the hydrogen atom which corresponds to the minimal geometry after the hydrogen escaped. From our calculations we conclude that the cage slightly expands (by less than 2%) due to the presence of the HCl molecule and the hydrogen angular position does not influence the cage size.

The normal vibrational frequencies of the cage are also almost independent of the rotational excitations of the embedded HCl molecule. The cage normal motions are schematically depicted in Fig. 3. The first three modes (T_{1u}) in descending order of normal frequencies are the translational modes of the center of mass of the HCl molecule. The next normal mode (A_g) corresponds to the totally symmetric breathing of the cage. The next quintet (H_g) is the symmetric stretch of the cage. Then, a triplet (T_{2u}) of the antisymmetric stretch of the cage follows. Up to this last triplet the perpendicular motion of the cage atoms with respect to the surface of the hydrogenic sphere dominates. The following motions of the cage are tangential to the sphere. The next quadruplet (G_u) is a double shear and the following quintet (H_g) is a single shear. Then, with almost degenerate energies a triplet (T_{1u}) and a quadruplet (G_g) follow. The triplet is a double torsion and in the quadruplet the argons compresses at one side of the shell. Finally, the last quintet (H_u) follows, which is a single torsion.

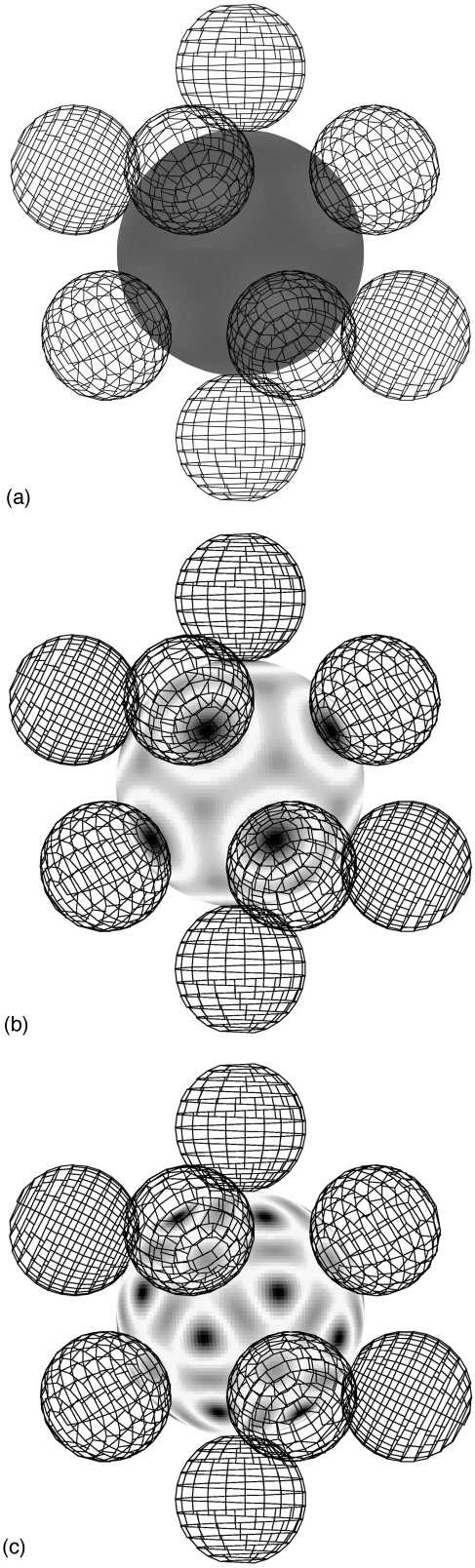

FIG. 2. Initial rotational wave functions of HCl molecules embedded in the center of an icosahedral cluster of 12 Ar atoms. (a), (b), and (c) show the three lowest rotational states within the totally symmetric A_g representation ($J=0,6,10$). The shadowing on the inner spheres corresponds to the probability of a certain orientation of the HCl molecule. The size of the inner spheres is, for the sake of clarity, artificially expanded. The outer spheres represent the Ar atoms with effective radii corresponding to Ar–H collision energy of 4 eV.

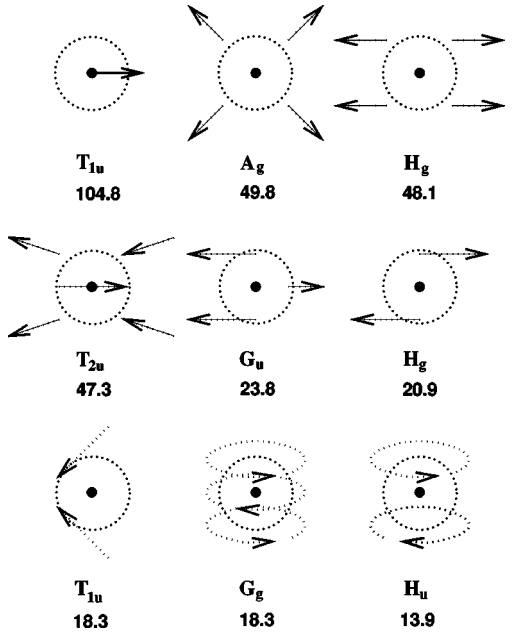

FIG. 3. Normal modes of vibration of the Ar atoms and of the HCl center of mass. The vibrational modes are schematically represented while the labels give the irreducible representation of the icosahedral point group (I_h) together with the harmonic frequency (in cm^{-1}).

B. Rotational control of wave packet dynamics

The dynamics of the HCl photodissociation process in the Ar_{12} cage and primarily of the hydrogen motion is crucially influenced by the initial hydrogen rotational state. In the following sections we examine the dynamics originating from the first three rotational states of the A_g symmetry ($J=0$, 6, and 10).

1. Dynamics of the hydrogenic radial motion

The photodissociation process is dominated by the large hydrogen excess energy and by cage constraints. Bifurcations of the hydrogen radial wave functions are observed upon collisions with the solvent cage. Direct cage exit, delayed cage exit with one or two collisions with the cage, and a temporary trapping are the four main branches of the process. In terms of schematic trajectories these four processes are illustrated in Fig. 4. In the case of direct dissociation, the hydrogen atom practically does not interact with the cage. If the hydrogen only grazes a cage atom and continues to dissociate with a slightly changed direction of its velocity we speak about dissociation delayed by one collision. If the hydrogen is reflected by a cage atom back to the cluster and escapes only during the second collision with the cage we speak about dissociation delayed by two collisions. Finally, if the hydrogen loses enough energy in the collision with the cage it can be temporarily trapped in the space between the chlorine and the argon shell. The relative occurrence of these four processes strongly depends on the initial angular positions of the hydrogen atom and, consequently, on the initial rotational state.

Let us now proceed to a more detailed analysis of the hydrogen wave function dynamics. This analysis is based on plots of the time evolution of the radial probability distributions $\Sigma_{J,N}|\chi_{J,N}(\rho,t)|^2$ depicted in Fig. 5. Starting from the ground rotational state [see Fig. 5(a)] dissociation delayed by one collision and direct dissociation are the dominant processes. Still, we can identify a small part of the wave packet which collides twice with the cage, and a minor tail of the temporarily trapped hydrogen. If the photodissociation process starts from the $J=6$ state where the hydrogen is preferentially directed toward the cage atoms, the two-collision process and direct dissociation dominate [see Fig. 5(b)]. A minor part of the temporarily trapped hydrogen is observed for $J=6$, too, with a longer lifetime than in the $J=0$ case. This behavior differs significantly from the previous case of the initial rotational ground state. If the $6J=10$ state where the hydrogen prefers positions toward the holes in the argon shell is initially populated, direct dissociation is a strongly dominant process [see Fig. 4(c)]. The two-collision process and temporary trapping are also observed but are relatively insignificant. This is again very different from the two previous cases. In summary, we observe a strong and significant rotational effect. The discrimination between the four photodissociation processes is, however, slightly blurred due to the finite widths of the initial angular distributions (see Fig. 2).

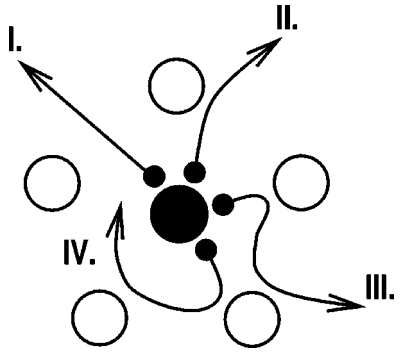

FIG. 4. Schematic illustration of the four possible reaction channels upon photolysis of HCl in $HCl@Ar_{12}$: (I) direct cage exit of the hydrogen, (II) cage exit delayed by one grazing collision, (III) cage exit delayed by two collisions, and (IV) temporarily trapped hydrogen inside the Ar solvent cage.

2. Population of the hydrogen inside the cage

The effect of the rotational control can be quantified in several ways. One option is to evaluate the temporary population of the hydrogen inside the cluster, which is in principle directly measurable by a pump–probe experiment. In our calculations it can be obtained as the part of the three-dimensional wave function of the hydrogen atom which remains inside the argon cluster. For this we integrate the square of the hydrogen wave function from 0 to 3.75 Å, which is the initial equilibrium distance of cage atoms from the center of the cluster.

The time-dependent hydrogen populations inside the cage for the three initial rotational states are depicted in Fig. 6. A fast population decay follows after reaching the cage at about 10 fs. First, we discuss the case of the initial ground rotational state. In this case 75% of the hydrogen density escapes during the first collision with the cage. Then, for about 20 fs an exponential decrease follows during which another 15% of the hydrogen density disappears. Around

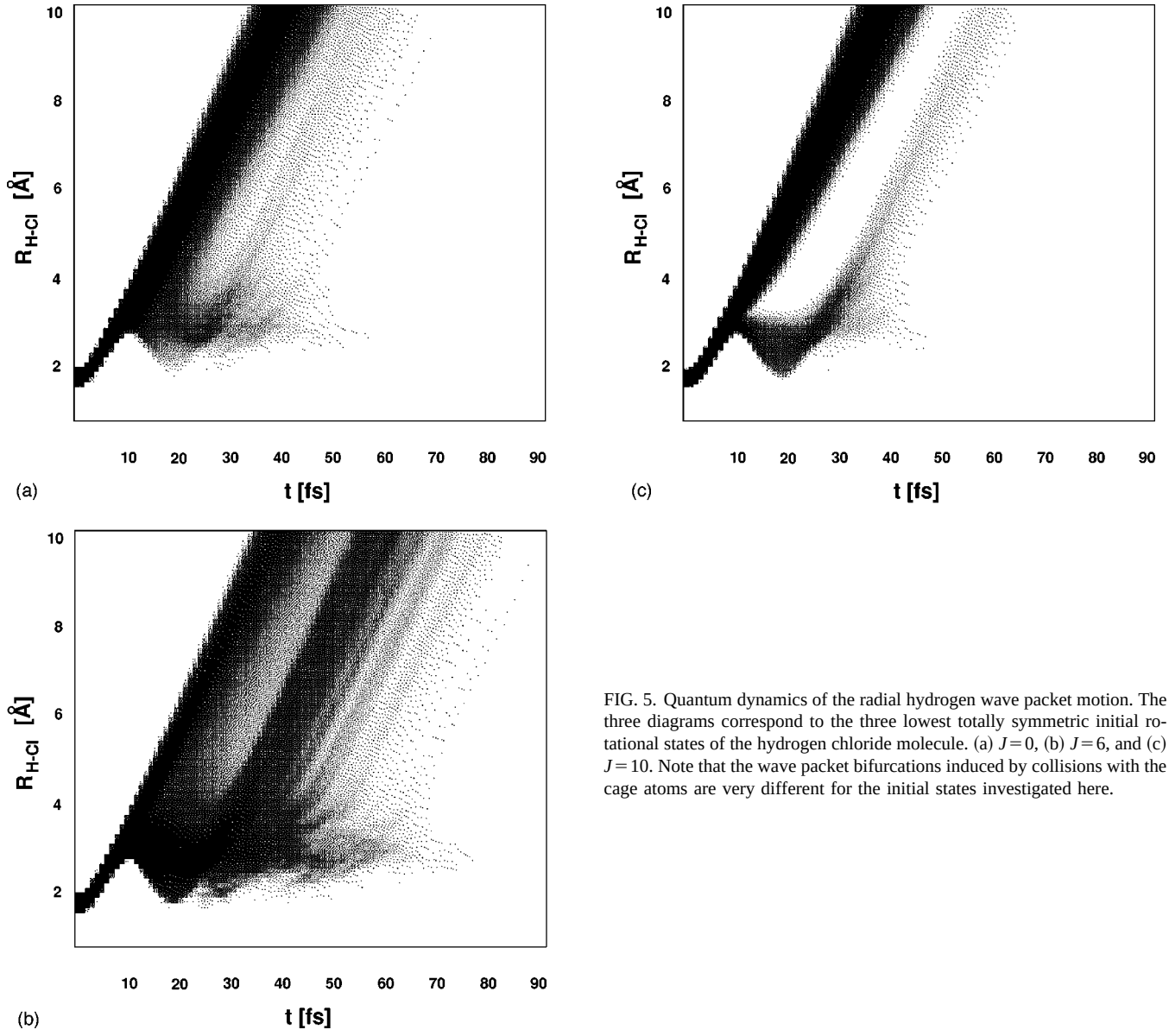

FIG. 5. Quantum dynamics of the radial hydrogen wave packet motion. The three diagrams correspond to the three lowest totally symmetric initial rotational states of the hydrogen chloride molecule. (a) $J=0$, (b) $J=6$, and (c) $J=10$. Note that the wave packet bifurcations induced by collisions with the cage atoms are very different for the initial states investigated here.

$t=30$ fs a small plateau on the curve appears which marks the second collision with the cage, after which an exponential decay continues. The temporarily trapped hydrogen which remains in the cluster even after the second collision practically entirely leaves the cluster before $t=80$ fs.

In the case of the $J=6$ state only about 30% of the hydrogen density escapes during the first collision with the cage. The following exponential decay decreases the population of the hydrogen inside the cage to 45% still before the second collision. As a result, the population of the hydrogen inside the cage between the first and the second collision is approximately 3.5 times larger than that resulting from the rotational ground state. A second collision with the cage occurs almost at the same time as in the previous case and it is accompanied by a significant step in the curve around 30 fs. After the second collision an exponential decay continues. As in the previous case, only two collisions can be distinguished, the second being much more delocalized in time. The tail of the temporarily trapped hydrogen vanishes around $t=110$ fs.

In the case of the $J=10$ state about 90% of the hydrogen density escapes by direct dissociation while only a minor part is reflected by the cage during the first collision. The decay of the population during the first collision is even faster than in the case of the ground initial rotational state. After a nearly flat segment on the curve a new significant decay begins after the second collision. The tail of the temporarily trapped hydrogen vanishes around $t=70$ fs. The population difference between the $J=10$ and $J=6$ cases is the largest. The corresponding populations differ by a factor of up to 4.5 after the first collision (at $t=18$ fs) and by more than a factor of 5 after the second collision ($t=40$ fs). Rotational preexcitation thus proves to be an efficient way to control temporary hydrogen populations inside the cage during photodissociation.

3. Kinetic energy distribution of the hydrogen atom

The rotational control mechanism can also be verified by energy domain measurements. Namely, it is the kinetic en-

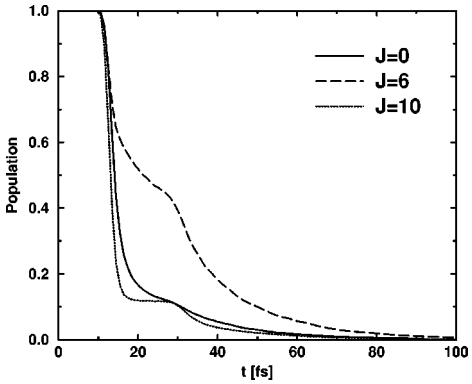

FIG. 6. Hydrogen cage exit upon photolysis of $HCl@Ar_{12}$: The curves show the probability of the hydrogen atom being inside the cage formed by the 12 Ar atoms. The differences in the three curves ($J=0,6,10$) establish the concept of rotational control of the dissociation yield.

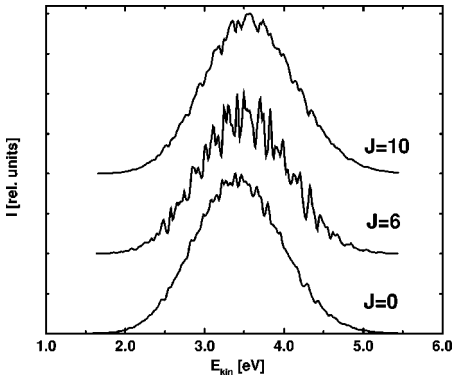

FIG. 7. Kinetic energy distribution of hydrogen atoms produced in photolysis of $HCl@Ar_{12}$: The curves show the probability distribution which is obtained as the Fourier transform of the H atom wave function for the three lowest totally symmetric initial rotational states ($J=0,6,10$). Note the different strength of the resonance pattern.

ergy distribution (KED) spectrum of the hydrogen atom which is directly observable, e.g., via time-of-flight measurements. In our simulation, it is obtained as a Fourier transform of the autocorrelation function of the three-dimensional hydrogen wave function. Note, that this is different from the photon absorption cross section which can be obtained as the Fourier transform of the autocorrelation function of the total time-dependent wave function.

The KED spectra for the three lowest totally symmetric rotational states are compared in Fig. 7. All three spectra show the same broad envelope which can be rationalized in terms of the reflection principle concerning the initial radial wave function.[82] The main difference between the three curves is in the fine structure corresponding to short-lived vibrational resonances. This structure is most pronounced in the case of the initial $J=6$ state where the population decay inside the cage is the slowest. Clearly, the longer time the hydrogen atom spends inside the cluster the more pronounced the vibrational peaks are. The vibrational spacing of the fine structure in the KED is approximately 0.2 eV, which corresponds to a vibrational period of 20 fs. This is the time necessary for the reflected fraction of the hydrogen wave function to return to the Franck–Condon region (see Fig. 5). We conclude, that control by rotational preexcitation has a qualitative effect on the vibrational structure of the KED spectrum.

V. CONCLUSIONS

In this work we have presented a novel approach to the rotational control of photolysis of small hydrogen-containing molecules embedded in cryogenic rare gas clusters. We have shown for the case of the HCl molecule in the icosahedral first argon solvation shell that photodissociation and caging can be strongly influenced by a rotational preexcitation of the host molecule. In particular, for the three lowest totally symmetric rotational states studied the relative propensities of the four observed dynamical channels—direct cage exit, cage exit delayed by one or two collisions, and temporary trapping, differ significantly. This has immediate consequences for observables both in the time and frequency domains. Namely, the temporary hydrogen populations inside the argon cage differ by up to a factor of 5 and the kinetic energy distributions of the hydrogen atoms show signatures of resonances of different strengths for the three investigated initial HCl rotational states. These vibrational resonances which reflect the partial caging by the argons might, however, be to a certain extent suppressed by higher temperatures and lowered cage symmetry expected under realistic experimental conditions.

From the methodological point of view it is of key importance that the initial state of the system, consisting of a cryogenic cage and a cold and almost freely rotating hydrogen atom, has to be treated quantum mechanically. On the other hand, due to the low energy content of the initial state a large degree of wave function separability can be plausibly assumed. Therefore, the initial wave functions have been constructed as products of cage and H–Cl harmonic ground vibrational functions and two-dimensional symmetry adapted rotational wave functions differing only slightly from the HCl free rotor functions. During the photodissociation process the system acquires a significant amount of kinetic energy and becomes more classical while at the same time more correlated. Two dynamical approaches have been applied, both treating the hydrogen dynamics by a fully quantal three-dimensional simulation accounting for the strong correlation between radial and angular degrees of freedom. Within the first method the cage dynamics has been described using classical mechanics while the second scheme treats it in an approximate quantum mechanical way. Due to a significant separation between hydrogen and cage dynamical time scales the two methods only slightly differ in predictions concerning the ultrafast dynamics of the hydrogen atom. On the other hand, the particular pattern of cage mode excitations by the photodissociating hydrogen is a much more subtle quantity and the two methods show nonnegligible differences. A detailed discussion of this topic is the subject of a forthcoming paper.

ACKNOWLEDGMENTS

We wish to thank Jörn Manz and Benny Gerber for stimulating discussions. This project is supported by a

Volkswagen Stiftung Grant No. I/72114 (B.S. and P.J.), by a Grant No. A4040706 from the Granting Agency of the Academy of Sciences of the Czech Republic (P.J.), and by the Deutsche Forschungsgemeinschaft through Program No. SFB 337 (B.S.).

[1] M. J. Elrod, D. W. Steyert, and R. J. Saykally, J. Chem. Phys. **94**, 58 (1991).
[2] M. J. Elrod, D. W. Steyert, and R. J. Saykally, J. Chem. Phys. **95**, 3182 (1991).
[3] M. J. Elrod, J. G. Loeser, and R. H. Saykally, J. Chem. Phys. **98**, 5352 (1993).
[4] L. Oudejans, K. Nauta, and R. E. Miller, J. Chem. Phys. **105**, 10410 (1996).
[5] D. J. Nesbitt, Faraday Discuss. **97**, 1 (1994).
[6] D. T. Anderson, S. Davis, and D. J. Nesbitt, J. Chem. Phys. **107**, 1115 (1997).
[7] J. M. Hutson, J. Chem. Phys. **89**, 4550 (1988).
[8] A. R. Cooper and J. M. Hutson, J. Chem. Phys. **98**, 5337 (1993).
[9] S. E. Choi and J. C. Light, J. Chem. Phys. **92**, 2129 (1990).
[10] P. P. Korambath, X. T. Wu, and E. F. Hayes, J. Phys. Chem. **100**, 6116 (1996).
[11] D. Xie and G. Yan, Int. J. Quantum Chem. **66**, 119 (1998).
[12] S. Liu, Z. Bacic, J. W. Moskowitz, and K. E. Schmidt, J. Chem. Phys. **100**, 7166 (1994).
[13] S. Liu, S. Bacic, J. W. Moskowitz, and K. E. Schmidt, J. Chem. Phys. **101**, 6359 (1994).
[14] P. Niyaz, Z. Bacic, J. W. Moskowitz, and K. E. Schmidt, Chem. Phys. Lett. **252**, 23 (1996).
[15] M. Lewerenz, J. Chem. Phys. **104**, 1028 (1996).
[16] B. L. Grigorenko, A. V. Nemukhin, and V. A. Apkarian, J. Chem. Phys. **104**, 5510 (1996).
[17] C. E. Dykstra, J. Chem. Phys. **108**, 6619 (1998).
[18] B. Schmidt and P. Jungwirth, Chem. Phys. Lett. **259**, 62 (1996).
[19] A. Ernesti and J. M. Hutson, J. Chem. Phys. **106**, 6288 (1997).
[20] A. Garcia-Vela, R. B. Gerber, D. G. Imre, and J. J. Valentini, Phys. Rev. Lett. **71**, 931 (1993).
[21] A. Garcia-Vela, R. B. Gerber, and U. Buck, J. Phys. Chem. **98**, 3518 (1994).
[22] A. Garcia-Vela and R. B. Gerber, J. Chem. Phys. **103**, 3463 (1995).
[23] A. Garcia-Vela, J. Chem. Phys. **108**, 5755 (1998).
[24] T. Schroeder, R. Schinke, M. Mandziuk, and Z. Bacic, J. Chem. Phys. **100**, 7239 (1994).
[25] T. Schroeder, R. Schinke, and Z. Bacic, Chem. Phys. Lett. **235**, 316 (1995).
[26] E. Narevicius, D. Neuhauser, H. J. Korsch, and N. Moiseyev, Chem. Phys. Lett. **276**, 250 (1997).
[27] M. Niv, A. I. Krylov, and R. B. Gerber, Faraday Discuss. **108**, 243 (1997).
[28] A. I. Krylov and R. B. Gerber, J. Chem. Phys. **106**, 6574 (1997).
[29] I. H. Gersonde and H. Gabriel, J. Chem. Phys. **98**, 2094 (1993).
[30] B. Schmidt, Chem. Phys. Lett. (submitted).
[31] M. Monnerville and B. Pouilly, Chem. Phys. Lett. **294**, 473 (1998).
[32] F. Neugebauer and V. May, Chem. Phys. Lett. **289**, 311 (1998).
[33] J. Manz, B. Schmidt, and P. Saalfrank, J. Chem. Soc., Faraday Trans. **93**, 957 (1997).
[34] B. Schmidt, P. Jungwirth, and R. B. Gerber, in *Femtochemistry*, edited by M. Chergui (World Scientific, River Edge, NJ, 1996), p. 637.
[35] R. J. Hinde, Chem. Phys. Lett. **289**, 67 (1998).
[36] P. Jungwirth, Chem. Phys. Lett. **289**, 324 (1998).
[37] R. L. van der Waal, J. L. Scott, and F. F. Crim, J. Chem. Phys. **92**, 803 (1990).
[38] F. F. Crim, J. Phys. Chem. **100**, 12725 (1996).
[39] I. Bar, Y. Cohen, D. David, T. Arusi-Parpar, S. Rosenwaks, and J. J. Valentini, J. Chem. Phys. **95**, 3341 (1991).
[40] E. Segev and M. Shapiro, J. Chem. Phys. **77**, 5604 (1982).
[41] V. Engel and R. Schinke, J. Chem. Phys. **88**, 6381 (1998).
[42] D. C. Imre and J. Zhang, Chem. Phys. **139**, 89 (1989).
[43] P. Jungwirth, P. Zdanska, and B. Schmidt, J. Phys. Chem. **102**, 7241 (1998).
[44] M. R. Hoare and P. Pal, in *Advances in Physics*, edited by B. R. Coles (Taylor and Francis, London, 1975), Vol. 24, p. 645.
[45] B. Raoult, J. Farges, M. F. de Feraudy, and G. Torchet, Z. Phys. D **12**, 85 (1989).
[46] J. M. Hutson, J. Phys. Chem. **96**, 4237 (1992).
[47] K. P. Hubert and G. Herzberg, *Molecular Spectra and Molecular Structure, Constants of Diatomic Molecules* (Van Nostrand, New York, 1979).
[48] R. A. Aziz and M. J. Slaman, Mol. Phys. **58**, 679 (1986).
[49] E. F. van Dishoeck, M. C. van Hemert, and A. Dalgarno, J. Chem. Phys. **77**, 3693 (1982).
[50] V. Aquilanti, D. Cappelletti, V. Lorent, E. Luzzatti, and F. Pirani, J. Phys. Chem. **97**, 2063 (1993).
[51] M. H. Alexander, B. Pouilly, and T. Duhoo, J. Chem. Phys. **99**, 1752 (1993).
[52] R. W. Bickes, B. Lantszch, J. P. Toennies, and K. Walaschewski, Faraday Discuss. Chem. Soc. **55**, 167 (1973).
[53] D. Bassi, M. G. Dondi, F. Tommasini, F. Torello, and U. Valbusa, Phys. Rev. A **13**, 584 (1976).
[54] K. T. Tang and J. P. Toennies, Chem. Phys. **156**, 413 (1991).
[55] H. Partridge, D. W. Schwenke, and C. W. Bauschlicher, J. Chem. Phys. **99**, 9776 (1993).
[56] M. J. Frisch, G. W. Trucks, H. B. Schlegel, P. M. W. Gill, B. G. Johnson, M. A. Robb, J. R. Cheeseman, T. Keith, G. A. Peterson, J. A. Montgomery, K. Ragavachari, M. A. Al-Laham, V. G. Zakrzewski, J. V. Ortiz, J. B. Foresman, J. Cioslowski, B. B. Stefanov, A. Nanayakkara, M. Challacombe, C. Y. Peng, P. Y. Ayala, W. Chen, M. W. Wong, J. L. Andres, E. S. Repogle, R. Gomperts, R. L. Martin, D. J. Fox, J. S. Binkley, D. J. DeFrees, J. Baker, J. P. Stewart, M. Head-Gordon, M. C. Gonzales, and J. A. Pople, GAUSSIAN 94, (Gaussian, Inc., Pittsburgh, PA, 1995).
[57] T. H. Dunning, Jr., J. Chem. Phys. **90**, 1007 (1989).
[58] R. A. Kendall, T. H. Dunning, Jr., and R. J. Harrison, J. Chem. Phys. **96**, 6796 (1992).
[59] D. E. Woon and T. H. Dunning, Jr., J. Chem. Phys. **98**, 1358 (1993).
[60] J. P. Toennies, W. Welz, and G. Wolf, J. Chem. Phys. **71**, 614 (1979).
[61] H. Dubost, in *Inert Gases*, edited by M. L. Klein, *Series in Chemical Physics*, Vol. 34 (Springer, Berlin, 1984), Chap. 4.
[62] M. T. Bowers and W. H. Flygare, J. Chem. Phys. **44**, 1389 (1966).
[63] R. B. Gerber, V. Buch, and M. A. Ratner, J. Chem. Phys. **77**, 3022 (1982).
[64] F. A. Bornemann, P. Nettesheim, and Ch. Schütte, J. Chem. Phys. **105**, 1074 (1996).
[65] C. Schütte and F. A. Bornemann, Konrad-Zuse-Center, preprint SC-97-41, available through `http://www.zib.de`.
[66] P. Jungwirth and R. B. Gerber, J. Chem. Phys. **102**, 6046 (1995).
[67] P. Jungwirth and R. B. Gerber, J. Chem. Phys. **104**, 5803 (1996).
[68] P. Jungwirth, E. Fredi, and R. B. Gerber, J. Chem. Phys. **107**, 8963 (1997).
[69] E. Wigner, Phys. Rev. **40**, 749 (1932).
[70] E. J. Heller, J. Chem. Phys. **65**, 1289 (1976).
[71] M. Hillery, R. F. O'Connel, M. O. Scully, and E. P. Wigner, Phys. Rep. **106**, 122 (1984).
[72] M. P. Allen and D. J. Tildesley, *Computer Simulation of Liquids* (Clarendon, Oxford, 1987).
[73] P. Zdanska and P. Jungwirth (unpublished).
[74] H. W. Lee, Phys. Rep. **259**, 148 (1995).
[75] P. Nettesheim and C. Schütte, Konrad-Zuse-Center, preprint SC-97-42 , available through `http://www.zib.de`.
[76] R. Kosloff, J. Phys. Chem. **92**, 2087 (1988).
[77] U. Schmidt and J. Brickmann, Chem. Phys. **208**, 45 (1996).
[78] P. Nettesheim, F. A. Bornemann, B. Schmidt, and Ch. Schütte, Chem. Phys. Lett. **256**, 581 (1996).
[79] M. D. Feit, J. A. Fleck, Jr., and A. Steiger, J. Comput. Phys. **47**, 412 (1982).
[80] C. J. Bradley and A. P. Cracknell, *The Mathematical Theory of Symmetry in Solids* (Clarendon, Oxford, 1972).
[81] W. Prandl, P. Schiebel, and K. Wulf, Acta Crystallogr., Sect. A: Found. Crystallogr. **52**, 171 (1996).
[82] R. Schinke, *Photodissociation Dynamics* (Cambridge University Press, Cambridge, 1993).